Optimal Linear-Quadratic Missile Guidance Laws using Minimum-Variability method

Research Project

Author: Dor Bar-Yosef
Advisor: Prof. Tal Shima

The Cooperative Autonomous Systems (CASY) Lab
Faculty of Aerospace Engineering, Technion

June 16, 2026

Abstract

This project derives optimal guidance laws for interceptor missiles using the minimum variability control framework based on Linear-Quadratic optimal control theory. Two formulations are developed. The first minimizes body attitude variability relative to the Line-of-Sight, yielding Proportional Navigation with an effective gain of 2 that produces a constant lateral acceleration command independent of the weighting parameter. The second augments the state with the flight path angle and penalizes its deviation from a collision-course reference angle, producing a closed-form law involving hyperbolic functions of the time-to-go. Analysis of the limiting cases shows that the law recovers classical PN when both weights grow to infinity and exhibits Guidance-to-Collision behavior when both approach zero. The reference angle is obtained geometrically via a fourth-order polynomial in the time-to-go. The analytical solutions for the Guidance-To-Collision law are validated against numerical Riccati solvers through non-linear simulations.

Nomenclature

Symbols

a_x	Constant axial acceleration
a_T	Target acceleration
$\tilde{B}$	Effective scalar control gain
$\boldsymbol{D}$	Terminal projection (selection) vector
H	Hamiltonian
HE	Heading error
J	Performance index (cost function)
K	System dynamic parameter, $K = 1/(V_M\sqrt{\beta})$
N	Navigation gain
R	Relative range between missile and target
R_0	Initial relative range
t	Time
t_f	Final time
t_{go}	Time-to-go, $t_{go} = t_f - t$
u	Lateral acceleration control input
V_c	Closing velocity
V_{c_0}	Initial closing velocity
$V_{c_{eff}}$	Effective closing velocity
V_M, V_T	Missile and target velocity magnitudes
$\boldsymbol{x}$	State vector
y	Relative lateral separation
$\dot{y}$	Relative lateral velocity
z	Zero-Effort Miss (ZEM)
α	Cost function weighting factor for terminal miss distance
β	Cost function weighting factor for control effort
γ_M, γ_T	Flight path angles of the missile and target
θ	Missile body attitude angle relative to the Line-of-Sight (LOS)
θ_{com}	Commanded body attitude angle relative to the LOS
λ	LOS angle
$\boldsymbol{\lambda}$	Costate vector
λ_z	Scalar costate associated with variable z
ξ	Optimization parameter (reference collision-course angle)
σ	Target heading angle relative to LOS
ϕ	Missile heading angle relative to LOS
ϕ_r	Required heading angle relative to LOS for collision course

$\mathbf{\Phi}(t_f, t)$	State Transition Matrix (STM)

Acronyms

DRE	Differential Riccati Equation
FOV	Field of View
GTC	Guidance To Collision
LOS	Line Of Sight
LQ	Linear-Quadratic
LTI	Linear Time Invariant
PIP	Predicted Intercept Point
PNG/PN	Proportional Navigation Guidance
RIP	Required Intercept Point
STM	State Transition Matrix
TVC	Thrust Vector Control
ZEM	Zero Effort Miss

Introduction

Guidance laws for interception have been extensively researched over the past 80 years, with numerous strategies developed using classical control theory, geometric approaches, and modern techniques such as optimal control theory. Research has addressed diverse engagement scenarios, including constant-velocity and variable-speed agents, maneuvering targets, and both endoatmospheric and exoatmospheric vehicles. The well-known Proportional Navigation Guidance (PNG), which relies on the Parallel Navigation geometric principle, has been implemented and modified for all these engagement scenarios in numerous publications.

Many guidance laws have been derived using optimal control theory based on the classical Linear-Quadratic (LQ) performance index, which minimizes a combination of terminal miss distance and control effort. Gazit and Gutman [1] presented three different guidance laws for constant-accelerating missiles: two based on optimal control strategies (one for non-maneuvering targets and another formulated as a differential game for maneuvering targets), and a third employing geometrical Guidance-To-Collision (GTC) strategy, which steers the missile onto a collision course until interception. In subsequent work, Gazit [2] expanded on the GTC law and examined its similarities to PNG for constant-speed missiles. Baba *et al.* [3] formulated a generalized GTC law, simplified it to a linearized case, and compared both with PNG, demonstrating superior performance of the former. Several recent studies have advanced the GTC approach for various engagement scenarios. Kim *et al.* [4] derived an optimal GTC law for accelerating and decelerating targets, comparing it with traditional guidance laws and demonstrating its superiority using a proposed time-to-go prediction method. In subsequent work, Kim *et al.* [5] addressed exoatmospheric interceptors that accelerate and maneuver by changing thrust direction relative to the flight path, developing three GTC-based guidance methods and demonstrating the energy efficiency of one law and its similarity to True Proportional Navigation. Shima and Golan [6] employed Sliding Mode Control to develop Parallel Navigation and GTC laws for accelerating exoatmospheric interceptor missiles, demonstrating the broader capture zone of the GTC law compared to alternative strategies. Reisner and Shima [7] later developed a GTC law for exoatmospheric accelerating interceptors using optimal control theory with a terminal body angle constraint at interception. Following a different approach, Jung *et al.* [8] proposed a speed control method for achieving GTC. Unlike traditional guidance laws that steer the path angle to nullify heading error, this approach varies the interceptor's speed to nullify heading error, resulting in fuel-efficient, collision-course interception.

While many of the aforementioned studies utilize similar performance indices based on classical LQ formulations from optimal control theory, Weiss and Shima [9, 10] proposed a novel cost function formulation that derives a law minimizing both control command

variability and control effort through two-stage optimization. The resulting law, which enables mitigation of saturation effects, behaves like PNG with different navigation gains when the weighting factors in the cost function are taken to extremes. Similar results can be achieved using the method of Grinfeld and Ben-Asher [11], which minimizes the integral of the jerk (the rate of change of acceleration) rather than the integral of acceleration squared.

This project adopts the approach of Weiss and Shima [9, 10] with the aim of deriving novel guidance strategies using alternative LQ formulations.

1 Constant Missile attitude for exo-atmospheric engagement

Problem Introduction & Non-linear Kinematics

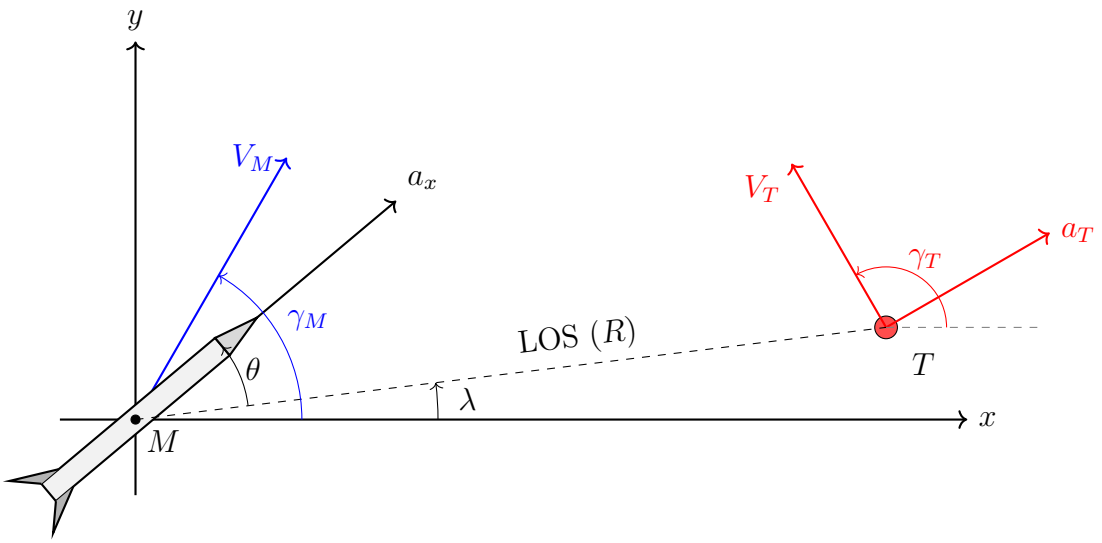

Figure 1: Engagement Geometry

Consider an exo-atmospheric interception scenario involving a missile (M) and a target (T). The missile is equipped with a Thrust Vector Control (TVC) system. The missile's total acceleration magnitude, denoted as a_x, is constant but is assumed to generate acceleration only in the missile's body axis direction. The missile maneuvers by tilting its body axis angle relative to the inertial reference frame. The misalignment between the body axis and the velocity vector direction γ_M creates a component of acceleration perpendicular to the velocity, allowing the missile to maneuver. Conversely, the component of acceleration aligned with the velocity changes the speed magnitude V_M.
The equations of motion governing the relative kinematics and missile dynamics in the polar coordinate system are given by:

$$\dot{R} = V_T \cos(\gamma_T - \lambda) - V_M \cos(\gamma_M - \lambda) \tag{1}$$

$$R\dot{\lambda} = V_T \sin(\gamma_T - \lambda) - V_M \sin(\gamma_M - \lambda) \tag{2}$$

$$\dot{V}_M = a_x \cos(\theta + \lambda - \gamma_M) \tag{3}$$

$$\dot{\gamma}_M = \frac{a_x \sin(\theta + \lambda - \gamma_M)}{V_M} \tag{4}$$

The angle θ is defined as the body axis angle relative to the **LOS**, thus the body attitude relative to the horizon would be $\theta + \lambda$. Note that $\dot{V}_M$ is non-zero because the thrust vector is not necessarily orthogonal to the velocity vector during maneuvers.

2 Linearized Formulation

We define the state vector $\boldsymbol{x}$ and the control input u as in the standard linearized model using relative separation:

$$\boldsymbol{x} = \begin{bmatrix} y \\ \dot{y} \end{bmatrix} \tag{5}$$

$$u = a_x \sin\theta \Rightarrow |u| \leq a_x \tag{6}$$

Using this formulation for the control input u the equations become completely linear. The linear state equations:

$$\dot{y} = x_2 \tag{7}$$

$$\ddot{y} = a_{T_\perp} - a_{M_\perp} = a_{T_\perp} - a_x \sin(\theta) = -u \tag{8}$$

where we assume that the Target does not maneuver.
The linear state-space representation $\dot{\boldsymbol{x}} = \boldsymbol{A}\boldsymbol{x} + \boldsymbol{B}u + \boldsymbol{G}w$:

$$\begin{bmatrix} \dot{y} \\ \ddot{y} \end{bmatrix} = \begin{bmatrix} 0 & 1 \\ 0 & 0 \end{bmatrix} \begin{bmatrix} y \\ \dot{y} \end{bmatrix} + \begin{bmatrix} 0 \\ -1 \end{bmatrix} u \tag{9}$$

3 Optimal Guidance Formulation

To derive the guidance law, we propose a cost function that balances the terminal miss distance against the variability of the control input. The performance index J is defined as:

$$J = \frac{1}{2} y^2(t_f) + \frac{\alpha}{2} \int_{t_0}^{t_f} (u(t) - \xi)^2 \, dt \tag{10}$$

where:

- $y(t_f)$ is the relative lateral separation at the final time (terminal miss distance), corresponding to the first element of the state vector.
- α is a weighting factor penalizing the control variability. As $\alpha \to \infty$, the control command approaches the value ξ.
- $u(t) = a_x \sin(\theta(t))$ is the control input.
- ξ is a static optimization parameter.

The parameter ξ represents a constant offset or reference command. The optimization process has two stages: first, the optimal control history $u^*(t)$ is derived assuming a fixed

ξ; subsequently, the parameter ξ itself will be optimized to minimize the global cost, thereby reducing the total control variability around the mean.

To simplify the optimal control problem, we introduce a change of variables that projects the current state onto the terminal manifold. This transformation allows us to express the problem in terms of the ZEM.
Let $\boldsymbol{\Phi}(t_f, t)$ be the State Transition Matrix (STM) of the homogeneous system $\dot{\boldsymbol{x}} = \boldsymbol{A}\boldsymbol{x}$. We define the scalar projected variable $z(t)$ as:

$$z(t) = \boldsymbol{D}^T \boldsymbol{\Phi}(t_f, t)\boldsymbol{x}(t) \tag{11}$$

where $\boldsymbol{D} = [1 \quad 0]$ is a selection vector that extracts the relative lateral position at the final time. Physically, $z(t)$ represents the predicted miss distance at time t_f if no further control actions or target maneuvers occur from time t onwards.
Differentiating $z(t)$ with respect to time, we obtain:

$$\dot{z}(t) = \boldsymbol{D}^T \left(\dot{\boldsymbol{\Phi}}(t_f, t)\boldsymbol{x}(t) + \boldsymbol{\Phi}(t_f, t)\dot{\boldsymbol{x}}(t) \right) \tag{12}$$

Recalling the property of the STM derivative $\dot{\boldsymbol{\Phi}}(t_f, t) = -\boldsymbol{\Phi}(t_f, t)\boldsymbol{A}$, and substituting the system dynamics $\dot{\boldsymbol{x}} = \boldsymbol{A}\boldsymbol{x} + \boldsymbol{B}u$, the free response terms cancel out:

$$\dot{z}(t) = \boldsymbol{D}^T \left(-\boldsymbol{\Phi}(t_f, t)\boldsymbol{A}\boldsymbol{x}(t) + \boldsymbol{\Phi}(t_f, t)(\boldsymbol{A}\boldsymbol{x}(t) + \boldsymbol{B}u(t)) \right) \tag{13}$$

$$\dot{z}(t) = \boldsymbol{D}^T \boldsymbol{\Phi}(t_f, t)\boldsymbol{B}u(t) \tag{14}$$

We define the effective control gain as $\tilde{B}(t) = \boldsymbol{D}^T \boldsymbol{\Phi}(t_f, t)\boldsymbol{B}$. Thus, the scalar dynamics become:

$$\dot{z}(t) = \tilde{B}(t)u(t) \tag{15}$$

At the final time t_f, the STM becomes the identity matrix $\boldsymbol{\Phi}(t_f, t_f) = \boldsymbol{I}$. Consequently, the transformed variable satisfies:

$$z(t_f) = \boldsymbol{D}^T \boldsymbol{I}\boldsymbol{x}(t_f) = y(t_f) \tag{16}$$

Substituting this into the performance index, the cost function can be rewritten in terms of z and u:

$$J = \frac{1}{2} z(t_f)^2 + \frac{\alpha}{2} \int_{t_0}^{t_f} (u(t) - \xi)^2 \, dt \tag{17}$$

This transformation reduces the problem dimensionality, as we now control a single scalar state z driven by u.

We solve the optimization problem for the scalar system $\dot{z} = \tilde{B}u$ with the cost function defined in the previous section. The Hamiltonian for the reduced system is:

$$H = \frac{\alpha}{2}(u - \xi)^2 + \lambda_z \tilde{B} u \tag{18}$$

where λ_z is the costate associated with the variable z.

The adjoint equation is:

$$\dot{\lambda_z} = -\frac{\partial H}{\partial z} = 0 \implies \lambda_z(t) = \text{constant} \tag{19}$$

Since the costate is constant, we denote $\lambda_z(t) = \lambda_z$.

The optimality condition requires $\frac{\partial H}{\partial u} = 0$:

$$\alpha(u - \xi) + \lambda_z \tilde{B} = 0 \implies u^*(t) = \xi - \frac{\lambda_z \tilde{B}(t)}{\alpha} \tag{20}$$

The transversality condition at the final time relates the costate to the terminal state:

$$\lambda_z(t_f) = \frac{\partial}{\partial \boldsymbol{z}(t_f)} \left(\frac{1}{2} z(t_f)^2 \right) = z(t_f) \tag{21}$$

Since λ_z is constant, $\lambda_z = z(t_f)$ for all t.

We can find the STM using the identity $\mathbf{\Phi}(t_f, t) = \mathcal{L}^{-1}\{s\mathbf{I} - \mathbf{A}\}$ for LTI systems.

$$\mathbf{\Phi}(t_f, t) = \mathcal{L}^{-1}\{ \begin{bmatrix} s & -1 \\ 0 & s \end{bmatrix}^{-1} \} = \mathcal{L}^{-1}\{ \begin{bmatrix} \frac{1}{s} & \frac{1}{s^2} \\ 0 & \frac{1}{s} \end{bmatrix} \} \tag{22}$$

$$\mathbf{\Phi}(t_f, t) = \begin{bmatrix} 1 & t_{go} \\ 0 & 1 \end{bmatrix} \tag{23}$$

Thus we can calculate $\tilde{B}(t)$:

$$\tilde{B}(t) = \begin{bmatrix} 1 & 0 \end{bmatrix} \begin{bmatrix} 1 & t_{go} \\ 0 & 1 \end{bmatrix} \begin{bmatrix} 0 \\ -1 \end{bmatrix} = -t_{go} \tag{24}$$

To find the closed-loop control law, we must eliminate the unknown terminal state $z(t_f)$ and express it in terms of the initial state $z(t_0)$. Integrating the state equation from the current time t_0 to t_f:

$$z(t_f) = z(t_0) + \int_{t_0}^{t_f} \dot{z}(\tau)\, d\tau = z(t_0) + \int_{t_0}^{t_f} \tilde{B}(\tau) u^*(\tau)\, d\tau \tag{25}$$

Substituting the expression for $u^*(\tau)$ from Eq. (20):

$$z(t_f) = z(t_0) + \int_{t_0}^{t_f} \tilde{B}(\tau) \left(\xi - \frac{\lambda_z \tilde{B}(\tau)}{\alpha} \right) d\tau \tag{26}$$

$$z(t_f) = z(t_0) - \xi \int_{t_0}^{t_f} (t_f - \tau)\, d\tau - \frac{z(t_f)}{\alpha} \int_{t_0}^{t_f} (t_f - \tau)^2\, d\tau \tag{27}$$

$$z(t_f) = z(t_0) - \xi \frac{t_f^2}{2} - \frac{z(t_f)}{\alpha} \frac{t_f^3}{3} \tag{28}$$

Solving for the terminal miss distance $z(t_f)$:

$$z(t_f) = \frac{z(t_0) - \xi \frac{t_f^2}{2}}{1 + \frac{1}{\alpha} \frac{t_f^3}{3}} \tag{29}$$

Finally, substituting the new $z(t_f)$ back into the control equation (20), we obtain the optimal guidance law:

$$\boxed{u^*(t) = \xi + \frac{z(t_0) - \xi \frac{t_f^2}{2}}{\alpha + \frac{t_f^3}{3}} t_{go}} \tag{30}$$

3.1 Optimization of Parameter ξ

The final step in the guidance loop is the determination of the optimal static offset ξ. This parameter is chosen to minimize the total cost J by setting $\frac{\partial J}{\partial \xi} = 0$. In a real-time implementation, ξ can be updated at each time step or computed once based on the initial engagement geometry to ensure the global minimum variability of the control effort. Having derived the structure of the optimal control law for a fixed ξ, we now determine the optimal value of this parameter to minimize the global cost function.

First, we substitute the optimal control law $u^*(t)$ back into the original cost function J. The integral term becomes:

$$\frac{\alpha}{2}\int_{t_0}^{t_f}(u^*(t)-\xi)^2\,dt = \frac{\alpha}{2}\int_{t_0}^{t_f}\left(\frac{z(t_0)-\xi\frac{t_f^2}{2}}{\alpha+\frac{t_f^3}{3}}t_{go}\right)^2 dt \tag{31}$$

The terminal cost term can be rewritten using equation (28) as:

$$\frac{1}{2}z^2(t_f) = \frac{1}{2}\left(\frac{z(t_0)-\xi\frac{t_f^2}{2}}{1+\frac{1}{\alpha}\frac{t_f^3}{3}}\right)^2 \tag{32}$$

Combining these, the total cost J is expressed as a function of the parameter ξ:

$$J^*(\xi) = \frac{1}{2}\left(\frac{z(t_0)-\xi\frac{t_f^2}{2}}{1+\frac{1}{\alpha}\frac{t_f^3}{3}}\right)^2 + \frac{\alpha}{2}\int_{t_0}^{t_f}\left(\frac{z(t_0)-\xi\frac{t_f^2}{2}}{\alpha+\frac{t_f^3}{3}}t_{go}\right)^2 dt \tag{33}$$

To find the optimal bias ξ^*, we minimize $J(\xi)$ by setting the partial derivative with respect to ξ to zero:

$$\frac{\partial J^*}{\partial \xi} = \frac{\partial}{\partial \xi}\left[\frac{1}{2}\left(\frac{z(t_0)-\xi\frac{t_f^2}{2}}{1+\frac{1}{\alpha}\frac{t_f^3}{3}}\right)^2\right] + \frac{\alpha}{2}\int_{t_0}^{t_f}\frac{\partial}{\partial \xi}\left[\left(\frac{z(t_0)-\xi\frac{t_f^2}{2}}{\alpha+\frac{t_f^3}{3}}t_{go}\right)^2\right]dt = 0 \tag{34}$$

Where we can take the derivative inside the integral since it is finite.

The derivation yields the following solution:

$$-\left(z(t_0)-\xi\frac{t_f^2}{2}\right)\frac{t_f^2}{2}\cdot\frac{\alpha}{\alpha+\frac{t_{go}^3}{3}} = 0 \implies \boxed{\xi^* = \frac{z(t_0)}{\frac{t_f^2}{2}}} \tag{35}$$

3.2 Complete Guidance strategy

Using the derivations above, in particular eqs. (30) , (35), yields the simple control strategy:

$$\boxed{u^*(t) = \frac{2 \cdot z(t_0)}{t_f^2}} \tag{36}$$

We now have an open-loop control strategy which depends only on the initial ZEM and the engagement duration. It is desirable to obtain a closed loop guidance command, thus integrating the state to some general time t yields the following relation:

$$z(t) = z(t_0) + \int_{t_0}^{t} \dot{z}(\tau)d\tau = z(t_0) + \int_{t_0}^{t} (\tau - t_f) \cdot \frac{2 \cdot z(t_f)}{t_f^2} d\tau \tag{37}$$

$$z(t) = z(t_0) \cdot \frac{t_{go}^2}{t_f^2} \rightarrow z(t_0) = z(t) \cdot \frac{t_f^2}{t_{go}^2} \tag{38}$$

Thus, the control strategy gets the simple, known form of Proportional Navigation with navigation effective gain of 2:

$$\boxed{u^*(t) = 2\frac{z(t)}{t_{go}^2}} \tag{39}$$

The results align with the theory, as PN with effective gain of 2 yields a constant acceleration perpendicular to the LOS (Constant attitude angle relative to the LOS) with a perfect hit-to-kill, zero-miss interception. The resulting strategy nullifies the cost function entirely, with no dependency on the weighting factor α, as can be seen also from the guidance command which does not depend on it.

4 MATLAB Implementation and Simulation Results

To validate the theoretical derivation, a numerical simulation was developed in MATLAB. The implementation bridges the gap between the linearized theoretical model and the non-linear kinematics of the actual engagement.

The simulation environment integrates the non-linear equations of motion derived in Section 2 using a fixed-step Euler solver. While the optimal control law was derived based on the linear state-space model where the state is $z(t)$, real-time implementation requires estimating $z(t)$ from non-linear measurements. In the linear domain, $z(t)$ is projected using the State Transition Matrix. In the non-linear engagement, we approximate the ZEM using the current kinematic observables. Assuming a constant velocity vehicle for simplicity, the ZEM is proportional to the LOS rate $\dot{\lambda}$:

$$\lambda = \tan\left(\frac{y}{x}\right) \approx \frac{y}{x} \tag{40}$$

$$\dot{\lambda} \approx \frac{d}{dt}(\frac{y}{x}) = \frac{\dot{y}x - \dot{x}y}{x^2} = \frac{\dot{y} \cdot V_c t_{go} - V_c \cdot y}{V_c^2 t_{go}^2} = \frac{1}{V_c t_{go}^2} \cdot \underbrace{(y + \dot{y} t_{go})}_{ZEM} \tag{41}$$

$$z(t) \approx \dot{\lambda} V_c t_{go}^2 \tag{42}$$

Where the closing velocity can be updated to the current velocity to account for the missile's acceleration, or taken as the average velocity of the missile during the engagement. Substituting this approximation into the derived optimal control law (Eq. 39), the linear acceleration command is converted into a body attitude command. Since the missile steers using the body angle θ to generate lateral acceleration $a_{M_\perp} \approx a_x \sin(\theta)$, the final non-linear guidance command becomes:

$$\theta_{cmd} = \arcsin\left(\frac{2V_c\dot{\lambda}}{a_x}\right) \tag{43}$$

To ensure physical realizability, the argument of the arcsine function is saturated to $[-1, 1]$.

To make a more accurate model and take into account the closing speed's variability, we can utilize the receding horizon method where the ZEM is calculated continuously through time with the instantaneous LOS, making the displacement y zero at all times. Thus, we can formulate our strategy:

$$u(t) = 2\frac{z(t)}{t_{go}^2} = 2\frac{\dot{y}t_{go}}{t_{go}^2} = 2\frac{\dot{y}}{t_{go}} = 2 \cdot \underbrace{\frac{\dot{y}}{R}}_{\dot{\lambda}} \cdot \frac{R}{t_{go}} \tag{44}$$

Thus, the guidance command which relies on non-linear measurements and considers the acceleration of the missile gets the following form:

$$u(t) = 2\dot{\lambda} \cdot \underbrace{\left(V_c + \frac{1}{2} a_x \cos(\gamma_M - \theta^* - \lambda) \cos(\gamma_M - \lambda) \cdot t_{go} \right)}_{V_{c_{eff}}} \tag{45}$$

Where θ^* is a constant which is calculated at the beginning from the initial geometry using the optimal parameter ξ^* as in eq. (35). This guidance command can be implemented similarly to eq.(43):

$$\theta_{cmd} = \arcsin\left(\frac{2V_{c_{eff}}\dot{\lambda}}{a_x} \right) \tag{46}$$

The time-to-go is a critical parameter for the guidance gains in numerous strategies and for the effective closing velocity in our case. Instead of a simple R/V_c approximation, we solve the quadratic equation of motion for a constant accelerating body along the Line of Sight to ensure accuracy throughout the boost phase.

To implement the time-to-go dependent guidance law, we must dynamically estimate the total time of flight, t_f. We evaluate the kinematics along the initial Line-of-Sight (LOS) vector. The relative closing velocity depends on the target velocity V_T and the missile velocity V_M, along with their respective initial flight path angles γ_T and γ_M. The rate of change of the relative range can be modeled by projecting the velocities onto the LOS. The missile velocity is time-varying due to the constant axial acceleration, given by:

$$V_M(t) = V_{M_0} + a_x \cos(\gamma_{M_0} - \theta^* - \lambda_0) \cdot t \tag{47}$$

where θ^* represents the optimal thrust angle offset which can be obtained from the parameter ξ^* as in the previous section, Eq. (35). Substituting this into the range rate equation yields the time-dependent closing velocity:

$$\dot{R}(t) = V_T \cos(\gamma_{T_0} - \lambda_0) - V_{M_0} \cos(\gamma_{M_0} - \lambda_0) - a_x \cos(\gamma_{M_0} - \theta^* - \lambda_0) \cos(\gamma_{M_0} - \lambda_0) \cdot t \tag{48}$$

We define the initial closing velocity as $V_{c_0} = -\left(V_T \cos(\gamma_{T_0} - \lambda_0) - V_{M_0} \cos(\gamma_{M_0} - \lambda_0)\right)$. Integrating the range rate over the differential time dt from $t = 0$ to the interception time t_f (where the final range is zero) provides the kinematic constraint:

$$0 - R_0 = -V_{c_0} t_f - a_x \cos(\gamma_{M_0} - \theta^* - \lambda_0) \cos(\gamma_{M_0} - \lambda_0) \cdot \frac{t_f^2}{2} \tag{49}$$

By rearranging the terms, we formulate a quadratic equation with respect to the time

of flight t_f:

$$\frac{a_x \cos(\gamma_{M_0} - \theta^* - \lambda_0)\cos(\gamma_{M_0} - \lambda_0)}{2} t_f^2 - V_{c_0} t_f - R_0 = 0 \tag{50}$$

Applying the standard quadratic formula, we obtain the analytical estimate for the interception time:

$$t_{f_{1,2}} = \frac{-V_{c_0} \pm \sqrt{V_{c_0}^2 + 2R_0 a_x \cos(\gamma_{M_0} - \theta^* - \lambda_0)\cos(\gamma_{M_0} - \lambda_0)}}{a_x \cos(\gamma_{M_0} - \theta^* - \lambda_0)\cos(\gamma_{M_0} - \lambda_0)} \tag{51}$$

The positive real root of this equation represents the physical time of flight required to nullify the relative range under the assumed acceleration profile.
Using the real-time values, we can obtain an estimate for the time-to-go:

$$t_{go_{1,2}} = \frac{-V_c \pm \sqrt{V_c^2 + 2R a_x \cos(\gamma_M - \theta^* - \lambda)\cos(\gamma_M - \lambda)}}{a_x \cos(\gamma_M - \theta^* - \lambda)\cos(\gamma_M - \lambda)} \tag{52}$$

4.1 Simulation Parameters

The engagement scenario is defined by a head-on intercept course against a faster target. The missile starts with an initial heading error relative to the collision triangle to force the guidance law to correct the trajectory. The simulation parameters are summarized in Table 1.

Table 1: Initial Engagement Parameters

Parameter	**Symbol**	**Value**
Longitudinal Acceleration	a_x	$100\,\mathrm{m/s^2}$
Missile Initial Velocity	V_{M_0}	$800\,\mathrm{m/s}$
Target Velocity	V_T	$1200\,\mathrm{m/s}$
Initial Range	R_0	$20\,\mathrm{km}$
Target Flight Path Angle	γ_{T_0}	150°
Heading Error	HE	-15°
Simulation Step Size	dt	$10^{-4}\,\mathrm{s}$

We compare the performance of the PN guidance law for four distinct values of the navigation gain N:

- $N = 2$: The optimal gain we achieved in the derivation for minimum variability of the body-attitude angle relative to the LOS throughout the engagement.
- $N = 3$: Classical optimal gain for a non-maneuvering target for minimum control effort. Lateral acceleration commands decrease linearly toward zero at the interception.

- $N = 6$: Aggressive maneuvering. The heading error nullifies early in the flight, leaving the body axis aligned with the LOS for the majority of the engagement.
- $N = 10$: Near-impulsive correction. The heading error is eliminated almost immediately after launch using all the acceleration capability to nullify it, after which the missile flies with its body towards the target to ensure zero angular acceleration for the LOS keeping it non-rotating.

4.2 Results and Analysis

4.2.1 Individual Engagement Trajectories

Figure 2 shows the individual interception trajectories for each navigation gain. The dashed black line represents the target path, the solid colored line is the missile trajectory, the dotted lines are instantaneous Lines-of-Sight, and the arrows indicate the body axis attitude.

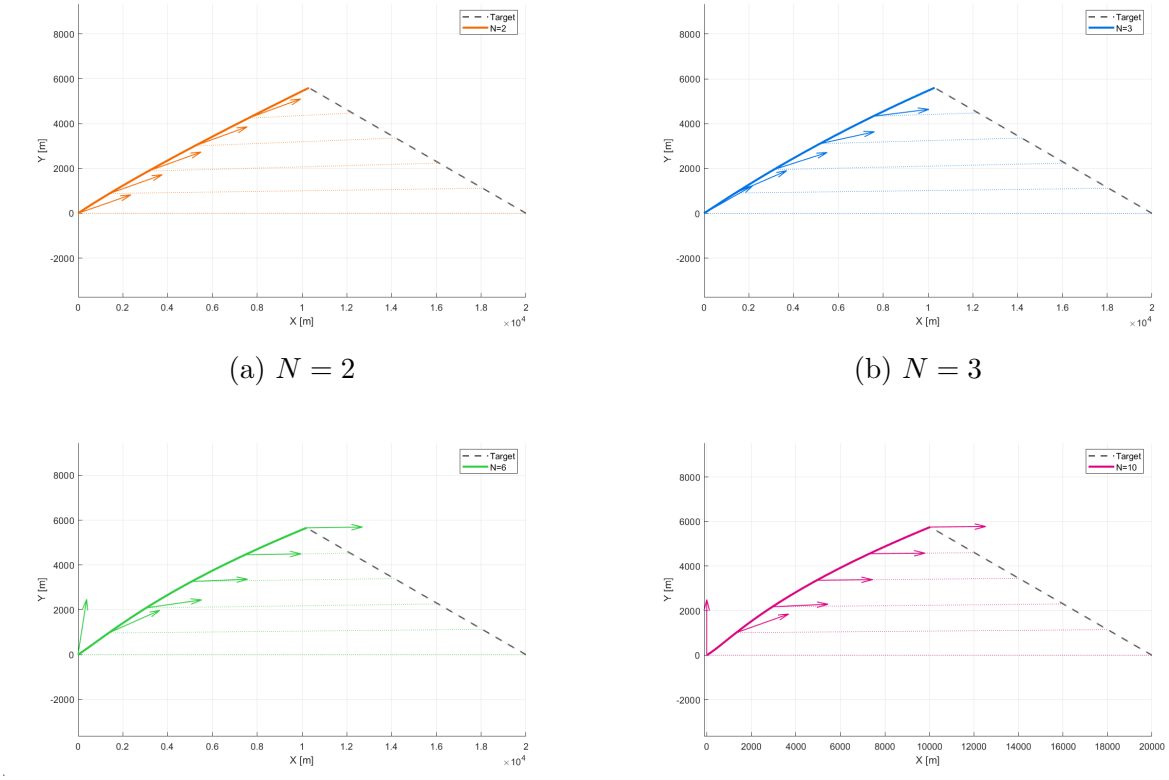

(a) $N = 2$ (b) $N = 3$

(c) $N = 6$ (d) $N = 10$

Figure 2: Individual interception trajectories for different navigation gain values.

The progressive effect of increasing the navigation gain is clearly visible, where higher gains produce a greater initial correction followed by a faster decrease of the body angle relative to the LOS. Moreover, a navigation gain of 2 seems to produce almost constant

body angle through the engagement, while increasing the gain causes more attitude variation of the missile. A combined overlay of all four trajectories is provided in Figure 3, allowing a direct comparison of the different trajectories. It is apparent that the lower navigation gains cause a faster interception of the target. The acceleration vector has more projection on the velocity with lower navigation gains, leading to higher velocity of the missile at the interception and reduced engagement time.

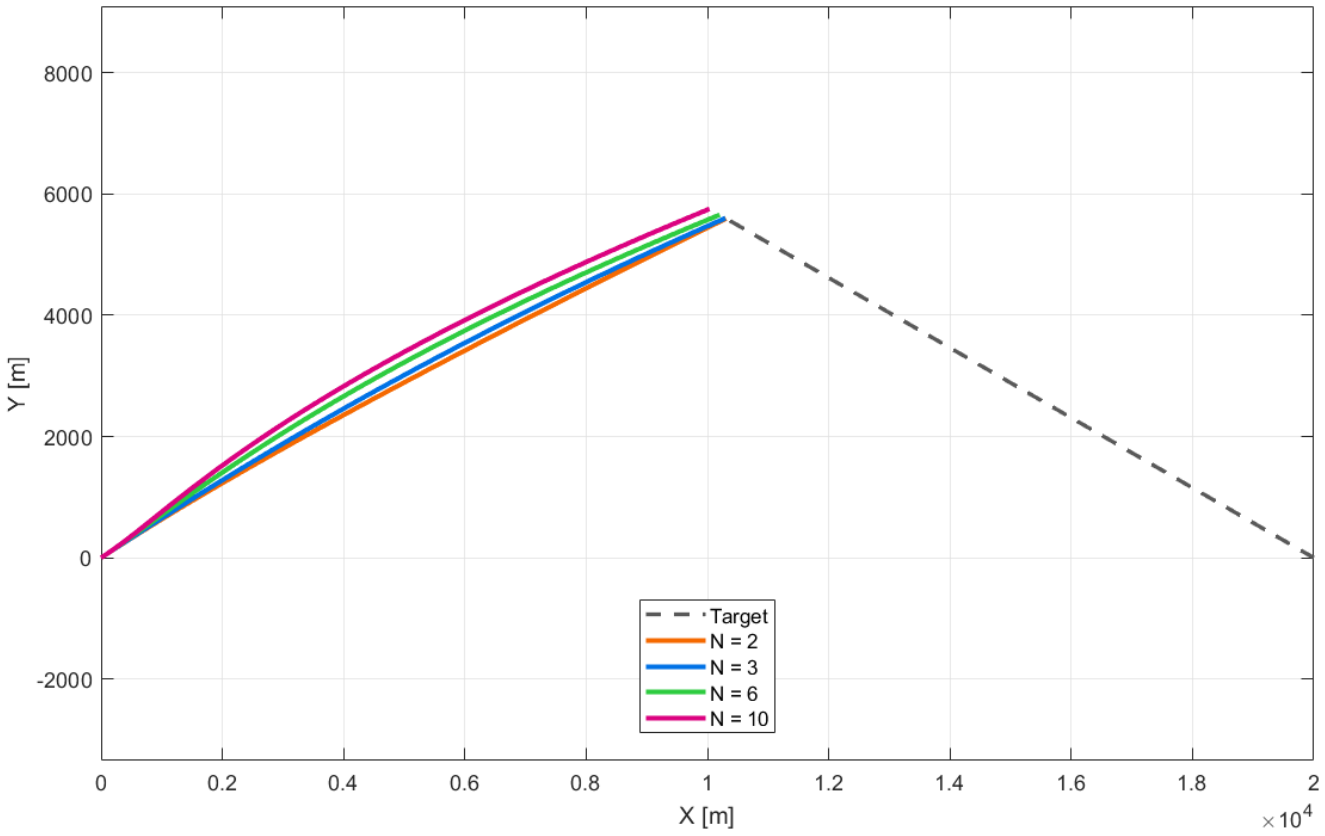

Figure 3: Overlay comparison of interception trajectories for different navigation gains

4.2.2 Body Angle Relative to the LOS

Figure 4 shows the body angle $\theta(t)$ relative to the LOS for all four gains on the same axes. The dashed line is the constant-attitude optimal angle calculated from the initial geometry of the engagement in the linear case. We can notice that our optimal strategy of PN with navigation gain of 2 manages to keep the missile attitude almost constant, and fairly close to the value calculated in the linear case. This is valuable since we can know the look angle relative to the missile body to take into account Field-of-View limits, missile body angle at interception *etc.*, apriori in the design stages.

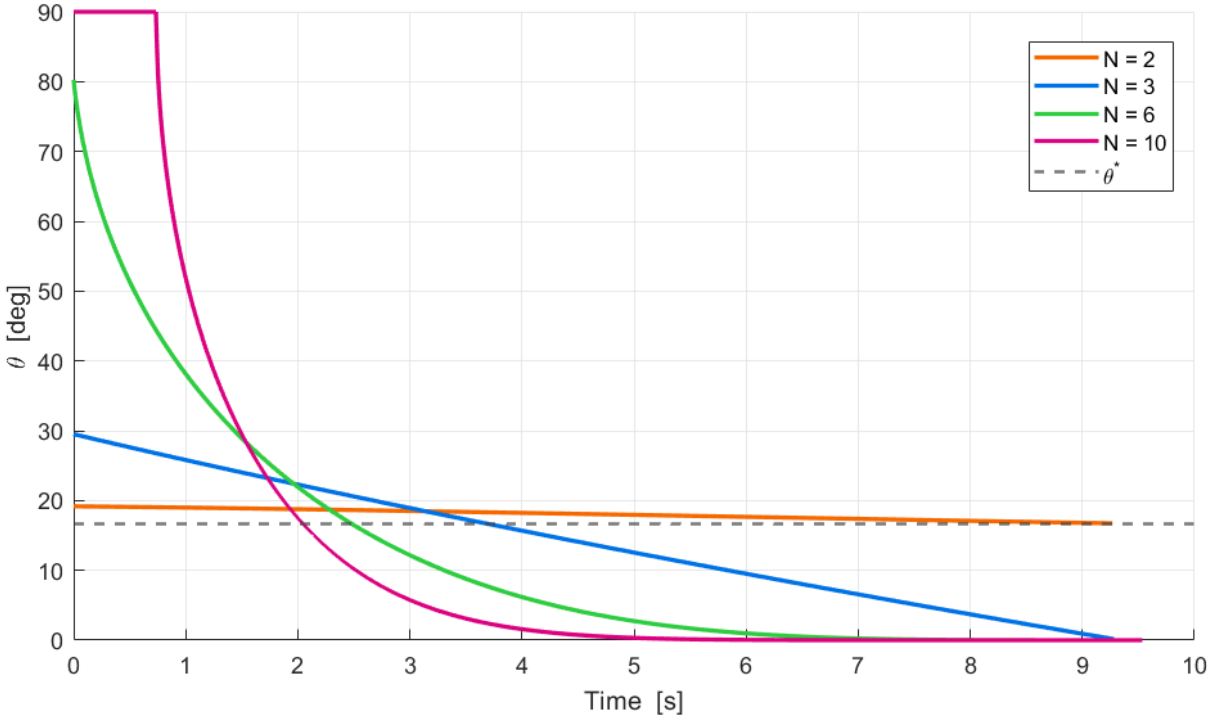

Figure 4: Body angle θ relative to the LOS vs. time for varying navigation gain N. The horizontal dashed line marks $\theta = 0$ (body on LOS).

4.2.3 Body-Axis Attitude Relative to the Inertial Frame

Figure 5 shows the inertial body attitude $\theta + \lambda$ throughout the engagement, i.e. the absolute pointing direction of the thrust vector with respect to the horizon. While Figure 4 captures the alignment with the LOS, this figure captures the total angular variation of the missile body in inertial space.

Higher navigation gains produce large range of variation for the inertial body angle, forcing the TVC actuator to exert greater effort and demanding more moment which may cause them to saturate. Lower navigation gains produce a narrower sweep of the body axis angle throughout the flight, becoming less vulnerable to earlier possible difficulties. This distinction is operationally significant for TVC missiles, where actuator deflection limits and structural bending loads are driven by the total angular range of body motion, which is minimized for navigation gain of 2, producing almost constant attitude missile with minimal actuator use.

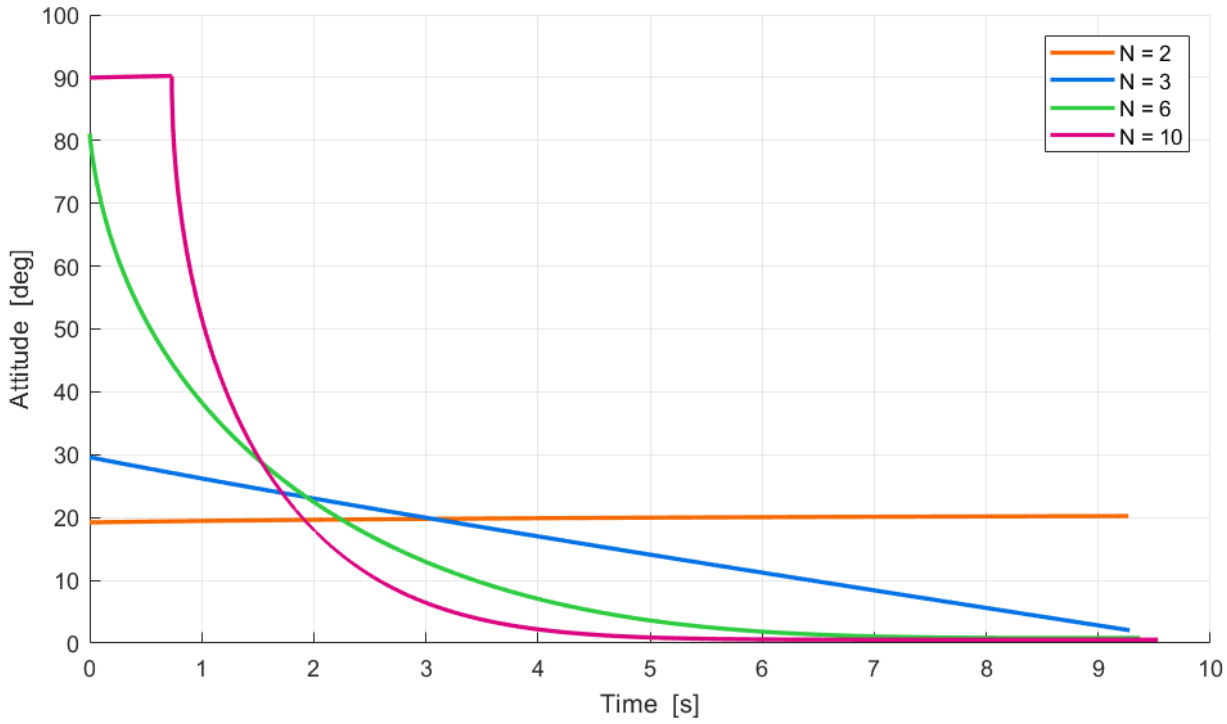

Figure 5: Inertial body attitude $\theta + \lambda$ for varying navigation gains.

4.2.4 Miss Distance and Accuracy

The miss distances for all tested navigation gains are summarized in Table 2. The theoretical miss distance for PN guidance is zero. Even for accelerating missiles, interception is guaranteed under ideal dynamics and perfect information. The miss distances in the simulation appeared to be only due to small numerical errors at the end of the simulation and quite small regardless.

Table 2: Miss Distance for Varying Navigation Gain

Navigation Gain N	**Miss Distance [cm]**
$N = 2$	2.71
$N = 3$	0.58
$N = 6$	11.05
$N = 10$	3.02

4.2.5 Time-to-Go Estimation and Velocity Profile

Figure 6 shows the missile speed and time-to-go estimate throughout the engagement. The velocity profile increases monotonically across all scenarios, reflecting the constant axial acceleration a_x. The rate of speed increase varies slightly with N since a larger body tilt redirects a greater fraction of the thrust laterally, reducing the axial component

and thus the speed increment per unit time. The time-to-go estimation remains accurate throughout, especially for the case where the assumption holds most, $N = 2$, validating the quadratic range-rate approximation used in the guidance loop.

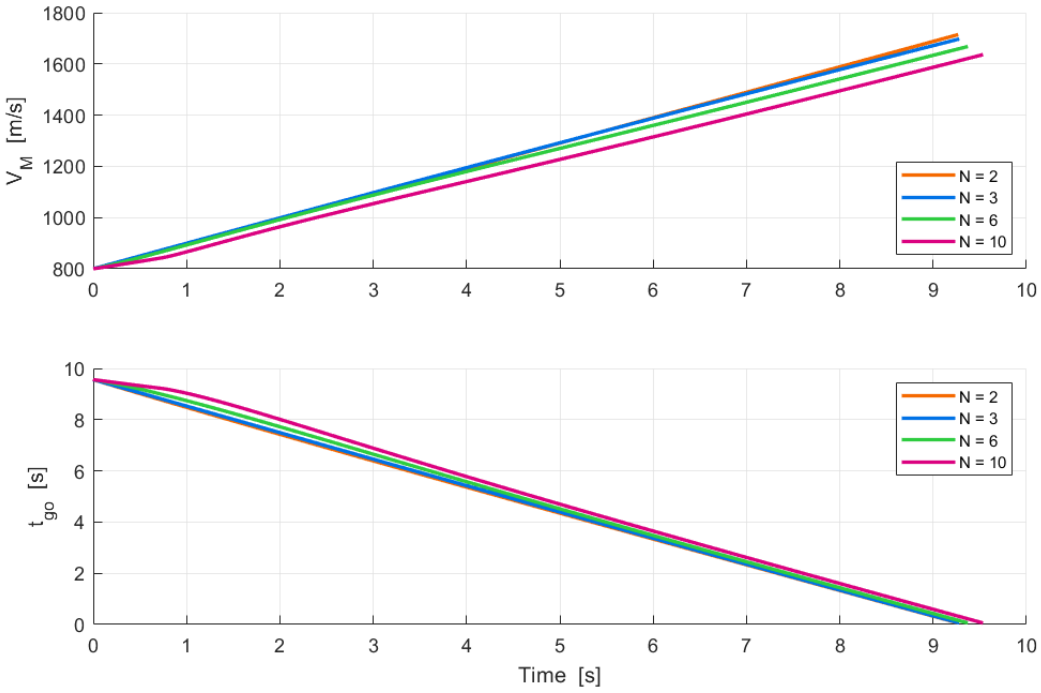

Figure 6: Missile velocity profile and time-to-go estimation for varying N.

5 Guidance-To-Collision for endo-atmospheric accelerating missiles

Problem Introduction & Non-linear Kinematics

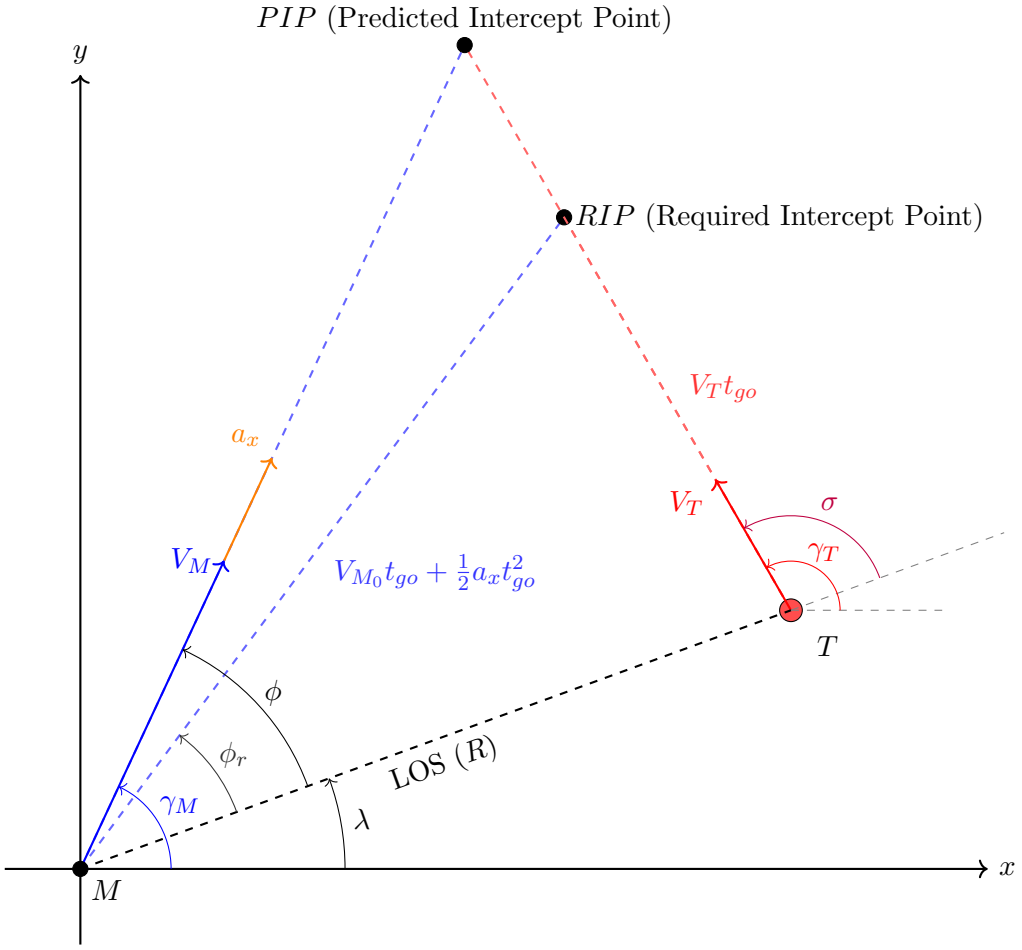

Figure 7: Engagement Geometry

Consider an endo-atmospheric interception scenario involving an accelerating guided missile (M) and a non-maneuvering target (T). The missile is propelled by a rocket motor that yields a constant axial acceleration magnitude, denoted as a_x, directed along the missile's longitudinal body axis. The missile maneuvers by deflecting its aerodynamic control surfaces to establish an angle of attack which generates aerodynamic lift, creating a dominant component of acceleration perpendicular to the velocity vector that allows the missile to steer. Concurrently, the projection of the constant axial acceleration a_x onto the velocity vector dictates the continuous increase in the missile's speed magnitude, V_M. The primary objective of the Guidance-to-Collision (GTC) strategy is to utilize this lateral acceleration to rapidly nullify any initial heading error, driving the missile onto a constant-bearing, straight-line collision triangle with the target, which is not as intu-

itive as in the constant speed interceptor case, where parallel navigation is a well-known guidance strategy that achieves the same geometry.

6 Linearized Formulation

To account for the missile's orientation and its alignment with a desired collision triangle, the previous kinematic model from the first problem is augmented to include the flight path angle γ_M as a third state. We define the augmented state vector $\boldsymbol{x}$ as:

$$\boldsymbol{x} = \begin{bmatrix} y \\ \dot{y} \\ \gamma_M \end{bmatrix} = \begin{bmatrix} x_1 \\ x_2 \\ x_3 \end{bmatrix} \tag{53}$$

Assuming a constant missile velocity V_M for the purpose of deriving the control law, the linearized dynamics relating the lateral acceleration command u to the flight path angle rate is $\dot{\gamma}_M = u/V_M$. The augmented state-space representation $\dot{\boldsymbol{x}} = \boldsymbol{A}\boldsymbol{x} + \boldsymbol{B}u$ becomes:

$$\begin{bmatrix} \dot{x}_1 \\ \dot{x}_2 \\ \dot{x}_3 \end{bmatrix} = \begin{bmatrix} 0 & 1 & 0 \\ 0 & 0 & 0 \\ 0 & 0 & 0 \end{bmatrix} \begin{bmatrix} x_1 \\ x_2 \\ x_3 \end{bmatrix} + \begin{bmatrix} 0 \\ -1 \\ \frac{1}{V_M} \end{bmatrix} u \tag{54}$$

7 Optimal Guidance Formulation

To derive a guidance law that not only guarantees a target intercept but also enforces a specific terminal geometry, we introduce a modified performance index. The new cost function heavily penalizes the terminal miss distance $x_1(t_f)$, weighs the total control effort, and introduces a running penalty on the deviation of the flight path angle $x_3(t)$ from a static reference angle ξ:

$$J = \frac{\alpha}{2}x_1^2(t_f) + \frac{\beta}{2}\int_{t_0}^{t_f} u^2(t)\,dt + \frac{1}{2}\int_{t_0}^{t_f} (x_3(t) - \xi)^2\,dt \tag{55}$$

where:

- α is the weighting factor for the terminal miss distance penalty.
- β is the weighting factor for the control effort penalty.
- ξ is the optimal reference angle required to maintain a collision triangle.

To find the closed-form analytical solution, we construct the Hamiltonian for the aug-

mented system. The Hamiltonian is defined as:

$$H = \frac{\beta}{2}u^2 + \frac{1}{2}(x_3 - \xi)^2 + \lambda_1 x_2 - \lambda_2 u + \lambda_3 \frac{u}{V_M} \tag{56}$$

where λ_1, λ_2, and λ_3 are the costates associated with the lateral separation, lateral velocity, and flight path angle, respectively.

Applying the optimality condition $\frac{\partial H}{\partial u} = 0$ yields the optimal control command:

$$\beta u - \lambda_2 + \frac{\lambda_3}{V_M} = 0 \implies u^*(t) = \frac{1}{\beta}\left(\lambda_2 - \frac{\lambda_3}{V_M}\right) \tag{57}$$

Next, we evaluate the adjoint equations $\dot{\lambda}_i = -\frac{\partial H}{\partial x_i}$ to find the costate dynamics:

$$\dot{\lambda}_1 = 0 \implies \lambda_1(t) = \text{constant} \tag{58}$$

$$\dot{\lambda}_2 = -\lambda_1 \tag{59}$$

$$\dot{\lambda}_3 = -(x_3 - \xi) \tag{60}$$

The transversality conditions at the final time t_f dictate the boundary values for the costates.

For the terminal miss distance penalty, we have:

$$\lambda_1(t_f) = \frac{\partial}{\partial x_1(t_f)}\left(\frac{\alpha}{2}x_1^2(t_f)\right) = \alpha x_1(t_f) \tag{61}$$

Since λ_1 is constant, this holds for all t. Integrating $\dot{\lambda}_2$ backward from its terminal condition $\lambda_2(t_f) = 0$ gives:

$$\lambda_2(t) = \alpha x_1(t_f)(t_f - t) = \alpha x_1(t_f) t_{go} \tag{62}$$

To solve for λ_3, we differentiate its adjoint equation, yielding $\ddot{\lambda}_3 = -\dot{x}_3$. Substituting the state dynamics $\dot{x}_3 = \frac{u}{V_M}$ and the optimal control $u^*(t)$, we obtain a second-order ordinary differential equation:

$$\ddot{\lambda}_3 - \frac{1}{\beta V_M^2}\lambda_3 = -\frac{1}{\beta V_M}\alpha x_1(t_f) t_{go} \tag{63}$$

We define the system dynamic parameter $K = \sqrt{1/(\beta V_M^2)}$. The characteristic equation is $r^2 - K^2 = 0$, yielding roots $r_{1,2} = \pm K$. The general solution for λ_3 in terms of time-to-go is composed of a homogeneous and a particular solution:

$$\lambda_3(t_{go}) = C_1 e^{K t_{go}} + C_2 e^{-K t_{go}} + V_M \alpha x_1(t_f) t_{go} \tag{64}$$

Applying the terminal boundary condition $\lambda_3(t = t_f) = 0$ reveals that $C_1 = -C_2$. Differentiating with respect to t_{go} and applying the condition $\lambda_3'(t = t_f) = x_3(t_f) - \xi$

allows us to solve for the integration constants:

$$C_1 = \frac{x_3(t_f) - \xi - V_M \alpha x_1(t_f)}{2K} \tag{65}$$

Substituting the constants back into the general solution yields the complete expression for the third costate:

$$\lambda_3(t_{go}) = \frac{x_3(t_f) - \xi - V_M \alpha x_1(t_f)}{K} \sinh(K t_{go}) + V_M \alpha x_1(t_f) t_{go} \tag{66}$$

Substituting $\lambda_2(t_{go})$ and $\lambda_3(t_{go})$ back into the optimality condition for $u^*(t)$, the linear t_{go} terms cancel out entirely, leaving the optimal control law as a function of the terminal states:

$$u^*(t) = \frac{V_M \alpha x_1(t_f) + \xi - x_3(t_f)}{\sqrt{\beta}} \sinh(K t_{go}) \tag{67}$$

where the expression $\beta K V_M$ reduces to $\sqrt{\beta}$:

To express the control law as a closed-loop feedback strategy, the unknown terminal state $x_3(t_f)$ must be resolved in terms of the current states. We determine the STM using the Laplace transform identity $\boldsymbol{\Phi}(t_{go}) = \mathcal{L}^{-1}\{(s\boldsymbol{I} - \boldsymbol{A})^{-1}\}$:

$$s\boldsymbol{I} - \boldsymbol{A} = \begin{bmatrix} s & -1 & 0 \\ 0 & s & 0 \\ 0 & 0 & s \end{bmatrix} \implies \boldsymbol{\Phi}(t_{go}) = \begin{bmatrix} 1 & t_{go} & 0 \\ 0 & 1 & 0 \\ 0 & 0 & 1 \end{bmatrix} \tag{68}$$

The terminal states are evaluated by integrating the states dynamics over the remaining flight time:

$$\boldsymbol{x}(t_f) = \boldsymbol{\Phi}(t_{go})\boldsymbol{x}(t) + \int_t^{t_f} \boldsymbol{\Phi}(t_f - \tau)\boldsymbol{B}u(\tau)d\tau \tag{69}$$

For the terminal flight path angle:

$$x_3(t_f) = x_3(t) + \int_0^{t_{go}} \frac{1}{V_M} u(\tau)\, d\tau \tag{70}$$

Substituting the derived $u^*(t)$ into the integral:

$$x_3(t_f) = x_3(t) + \frac{V_M \alpha x_1(t_f) + \xi - x_3(t_f)}{\sqrt{\beta} \cdot V_M} \int_0^{t_{go}} \sinh(K\tau)\, d\tau \tag{71}$$

Evaluating the integral yields $\frac{1}{K}(\cosh(K t_{go}) - 1)$. Recognizing the relation $\sqrt{\beta} K V_M = 1$,

the equation simplifies to:

$$x_3(t_f) = x_3(t) + (V_M \alpha x_1(t_f) + \xi - x_3(t_f))(\cosh(K t_{go}) - 1) \tag{72}$$

Expanding and isolating $x_3(t_f)$ provides the final closed-form resolution for the terminal flight path angle:

$$x_3(t_f) = \frac{x_3(t) + (V_M \alpha x_1(t_f) + \xi)(\cosh(K t_{go}) - 1)}{\cosh(K t_{go})} \tag{73}$$

Similarly, the equation for the terminal lateral separation:

$$x_1(t_f) = x_1(t) + x_2(t) \cdot t_{go} + \int_0^{t_{go}} -\tau \cdot u(\tau)\, d\tau \tag{74}$$

Substituting $u^*(t)$ into the integral:

$$x_1(t_f) = x_1(t) + x_2(t) \cdot t_{go} + \frac{V_M \alpha x_1(t_f) + \xi - x_3(t_f)}{\sqrt{\beta}} \underbrace{\int_0^{t_{go}} -\tau \cdot \sinh(K\tau)\, d\tau}_{I} \tag{75}$$

Isolating $x_1(t_f)$ gives us:

$$x_1(t_f) = \frac{x_1(t) + x_2(t) \cdot t_{go} + (\xi - x_3(t_f)) \cdot \frac{I}{\sqrt{\beta}}}{1 - V_M \alpha \frac{I}{\sqrt{\beta}}} \tag{76}$$

We can solve the system of equations for $x_1(t_f)$ and $x_3(t_f)$ in eqs.(73) and (77) and substitute them into the control command. The time-varying optimal control command $u^*(t)$ can be formulated entirely as a feedback law dependent only on current, measurable states.
The control strategy takes the following simple, analytical form:

$$u^*(t) = \frac{(V_M \alpha \cdot \overbrace{(x_1 + x_2 \cdot t_{go})}^{ZEM} + \xi - \gamma_M) \sinh(K t_{go})}{\sqrt{\beta} \cosh(K t_{go})(1 + V_M^2 \alpha t_{go}) - V_M^3 \alpha \beta \sinh(K t_{go})} \tag{77}$$

where ZEM is the Zero-Effort Miss. This explicit formulation eliminates the need for real-time numerical integration of the Riccati equations, significantly reducing computational load while maintaining mathematical optimality. Let us examine the following guidance law with its limiting cases:

Case 1: $\alpha, \beta \to \infty$ **with fixed ratio:** Let $\alpha = aL$ and $\beta = bL$ with $L \to \infty$, so that $K\,t_{go} = \frac{t_{go}}{V_M\sqrt{bL}} \to 0$. Expanding the hyperbolic functions in Taylor series and taking the limit yields:

$$u^*\Big|_{\alpha,\beta\to\infty} = \frac{3\,\dfrac{\alpha}{\beta}\,t_{go}\,(x_1 + t_{go}\,x_2)}{\dfrac{\alpha}{\beta}\,t_{go}^3 + 3} \tag{78}$$

Notably, the terminal angle constraint $(\xi - \gamma_M)$ drops out entirely, and the control depends only on the ZEM, weighted by the ratio α/β. In particular, when $\alpha/\beta \to \infty$, one recovers the classical PN form $u^* = 3\frac{ZEM}{t_{go}^2}$.

Case 2: $\alpha, \beta \to 0$ **with fixed ratio:** Let $\alpha = a\varepsilon$ and $\beta = b\varepsilon$ with $\varepsilon \to 0$. Now $K\,t_{go} \to \infty$, so $\tanh(K\,t_{go}) \to 1$. Since $\alpha \to 0$, the miss-distance terms vanish from the numerator, while the denominator behaves as $\sqrt{\beta}$. This gives:

$$u^*\Big|_{\alpha,\beta\to 0} \;\to\; \frac{\xi - \gamma_M}{\sqrt{\beta}} \tag{79}$$

The control is driven solely by the terminal impact-angle error $(\xi - \gamma_M)$, with the zero-effort-miss playing no role. The divergence as $1/\sqrt{\beta}$ reflects the vanishing penalty on control effort: the optimizer demands unbounded acceleration to enforce the angle constraint exactly. This limiting case exhibit Bang-Bang behavior: as $\beta \to 0$, the command saturates until the heading-angle error is nullified completely, after which the lateral acceleration drops to zero and the missile maintains a collision-course heading.

Case 3: $\beta \to 0$**,** α **fixed:** With $\beta \to 0$ and α held constant, we again enter the regime $K\,t_{go} \to \infty$ and $\tanh(K\,t_{go}) \to 1$. However, the finite α preserves the miss-distance terms:

$$u^*\Big|_{\beta\to 0} \;\to\; \frac{V_M\alpha\,(x_1 + t_{go}\,x_2) + (\xi - \gamma_M)}{\sqrt{\beta}\,(1 + V_M^2\alpha\,t_{go})} \tag{80}$$

This again diverges as $1/\sqrt{\beta}$, consistent with the removal of the control penalty. Unlike Case 2, both the miss-distance minimization and the impact-angle constraint remain active in the numerator, weighted by α. One can verify consistency: sending $\alpha \to 0$ in (80) recovers (79).

7.1 Optimization of parameter ξ

The optimization parameter ξ represents the ideal flight path angle γ_M^* required to achieve a straight-line intercept. Similar approach to previous problem for optimizing the parameter ξ results in an impractical guidance scheme to implement. Thus, we will continue in the geometric approach similarly to several publications in this topic [3, 7] and then validate the solution with optimal numerical results.
By applying the Law of Cosines to the collision triangle geometry, we can extract the time of flight for the GTC geometry by solving the following 4th-order polynomial equation:

$$\frac{1}{4}a_x^2 t_{go}^4 + a_x V_{M_0} t_{go}^3 + (V_{M_0}^2 - V_T^2) t_{go}^2 - 2RV_T \cos(\sigma) t_{go} - R^2 = 0 \tag{81}$$

where $\sigma = \gamma_T - \lambda$ is the target's flight path angle relative to the LOS.
The real and positive roots of this polynomial represent the optimal time-to-go which achieves Guidance-to-Collision triangles, denoted $t_{go_{opt}}$. The required heading of the missile relative to the LOS ϕ_r to achieve the triangle is then calculated as:

$$\phi_r = \tan^{-1}\left(\frac{V_T t_{go_{opt}} \sin(\sigma)}{V_T t_{go_{opt}} \cos(\sigma) + R}\right) \tag{82}$$

Finally, the optimal static offset ξ provided to the control law is defined as the sum of the instantaneous Line-of-Sight angle and the required heading:

$$\xi = \lambda + \phi_r \tag{83}$$

By achieving this angle earlier in the flight, the minimization of the heading angle running cost is guaranteed. Calculating this angle in a closed-loop throughout the engagement ensures interception even when the initial heading error is large.

8 MATLAB Implementation and Simulation Results

To validate the theoretical derivation of the guidance law, a numerical simulation was developed. The implementation bridges the gap between the linearized 3-state theoretical model and the non-linear kinematics of the engagement, while also verifying the analytical closed-form solution against a numerical Differential Riccati Equation (DRE) solver.
The simulation environment integrates the non-linear equations of motion using the `ode45` function in MATLAB. The implementation of the guidance law requires specific adaptations for real-time execution.
While the optimal control law $u^*(t)$ was derived using a linearized system, the real-time simulation operates in non-linear kinematics. The ZEM must be continuously estimated using non-linear measurements. As shown before in this project in section 4, the ZEM is formulated using the LOS rate $\dot{\lambda}$:

$$ZEM \approx \dot{\lambda} V_{c_{eff}} t_{go}^2 \tag{84}$$

$$V_{c_{eff}} = V_c + \frac{1}{2} a_x \cos(\phi) t_{go} \tag{85}$$

where $V_{c_{eff}}$ accounts for the missile's axial acceleration projected along the LOS. This ZEM approximation is directly substituted into the closed-form of the control law.
A critical component of this guidance strategy is the reference angle ξ. To avoid the heavy computational burden of solving coupled non-linear trigonometric equations at every time step, the geometric collision triangle was collapsed into a single 4th-order polynomial with respect to t_{go}. Finding the roots of the polynomial and taking the real positive one, the exact heading error ϕ_r required to close the triangle is calculated, and the static offset $\xi = \lambda + \phi_r$ is acquired for the law implementation. This ensures minimum variability of the flight path angle relative to the ideal trajectory and guarantees interception.

8.1 Simulation Parameters

Table 3: Engagement Parameters and Cost Weights

Parameter	**Symbol**	**Value**
Longitudinal Acceleration	a_x	$200\,\mathrm{m/s^2}$
Missile Initial Velocity	V_{M_0}	$800\,\mathrm{m/s}$
Target Velocity	V_T	$500\,\mathrm{m/s}$
Initial Range	R_0	$8000\,\mathrm{m}$
Target Flight Path Angle	γ_{T_0}	150°
Missile Flight Path Angle	γ_{M_0}	-10°

The engagement scenario is defined by a head-on intercept course against a target. The missile is given an initial heading error to force the guidance law to correct the trajectory and align the flight path angle γ_M with the reference ξ. The simulation parameters are summarized in Table 3.

8.2 Results and Analysis

8.2.1 Effect of Cost Function Weighting Parameters

The performance of the guidance law is critically dependent on the relative weighting between the terminal miss penalty (α), control effort penalty (β), and the running state cost. To demonstrate this sensitivity, multiple simulations were conducted with varying weight combinations while maintaining identical initial conditions.

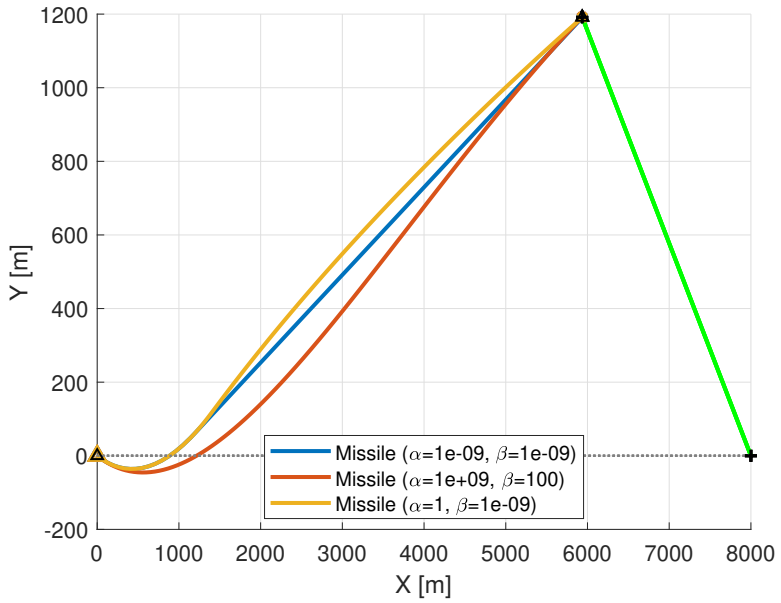

Figure 8: Missile trajectories for varying cost function weights

Figure 8 presents the missile trajectories under different weighting schemes. The first trajectory achieves GTC as both the terminal miss weight and control effort weight approach zero. The second trajectory yields the classical PN guidance law, and the third trajectory corresponds to the case where the terminal miss weight and the minimum variability weight are equal. For all engagements, the miss distance is negligible.

The flight path angle response, shown in Figure 9, reveals the true behavior of each guidance strategy. It can be observed that the GTC law maintains a constant heading angle toward collision, while the estimate of the parameter ξ converges to the optimal path angle once the missile reaches this angle. In the third scenario, the guidance scheme attempts to guarantee interception while minimizing the variability of the flight path angle, causing the missile to overcompensate with maximum acceleration to ensure minimal miss distance while remaining close to the optimal heading angle throughout the engagement.

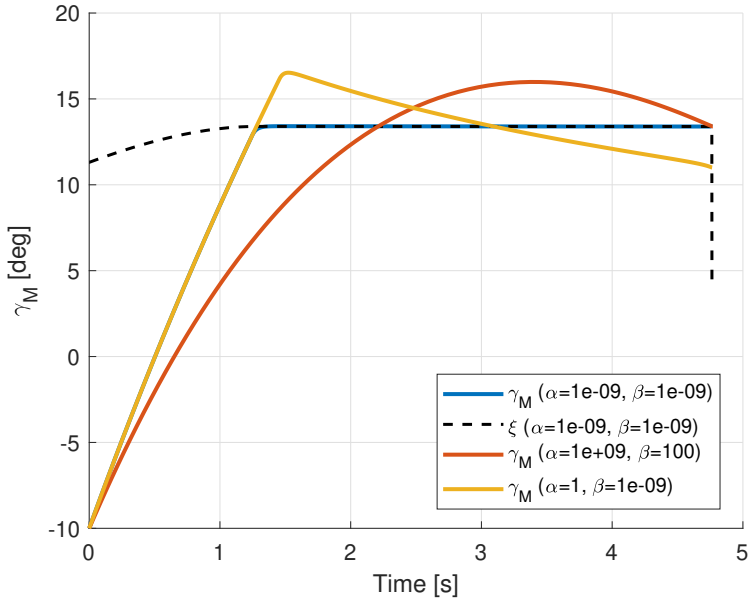

Figure 9: Flight path angle γ_M for different weighting parameters

Figure 10 illustrates the lateral acceleration command profiles corresponding to each weighting scheme. Aggressive weighting on state variability produces maximal initial acceleration commands with rapid decay to steady state, as required by GTC, while control-effort-dominant weights, such as those in the PN guidance law, yield smoother and more sustained command profiles. This demonstrates the fundamental trade-off between command variability and tracking performance inherent in the LQ formulation.

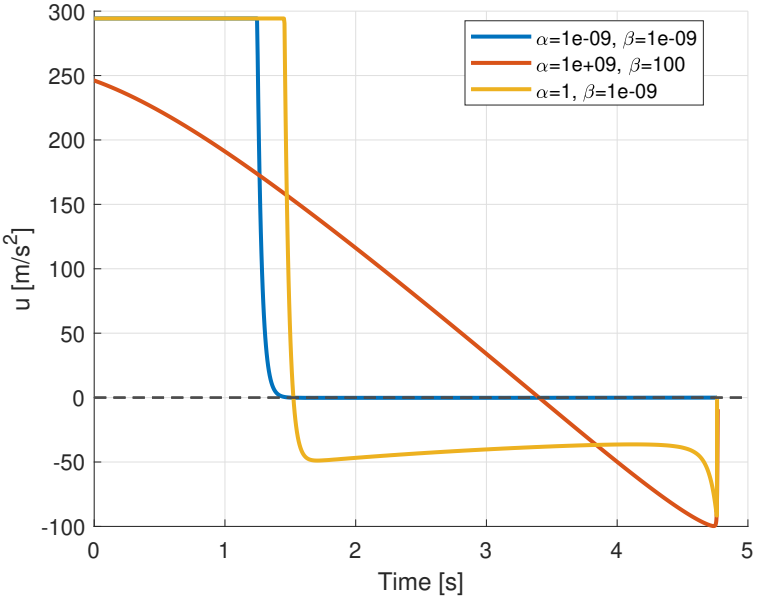

Figure 10: Lateral acceleration command profiles for different cost function weights

8.2.2 Analytical vs. Numerical Riccati Verification

To rigorously validate the closed-form analytical control law, the identical engagement scenario was simulated using a time-varying numerical DRE solver for a system that accounts for the missile's acceleration, as well as a numerical DRE solver for the original constant-velocity system used in this project. The system matrices $\boldsymbol{A}$, $\boldsymbol{B}$, $\boldsymbol{Q}$, and $\boldsymbol{S_f}$ were formulated for the 3-state augmented system, and MATLAB's `ode45` was employed to integrate the DRE backward in time-to-go, accounting for the velocity-dependent dynamics in the $\boldsymbol{B}$ matrix. This numerical solution provides the benchmark against which the analytical derivation is validated.

Figure 11 demonstrates perfect agreement between the analytical and numerical solutions of the GTC strategy. Both methods produce identical interception geometries, confirming that the closed-form solution captures the complete optimal behavior without approximation. The overlapping trajectories validate the mathematical derivation and demonstrate that real-time implementation is feasible without numerical integration overhead.

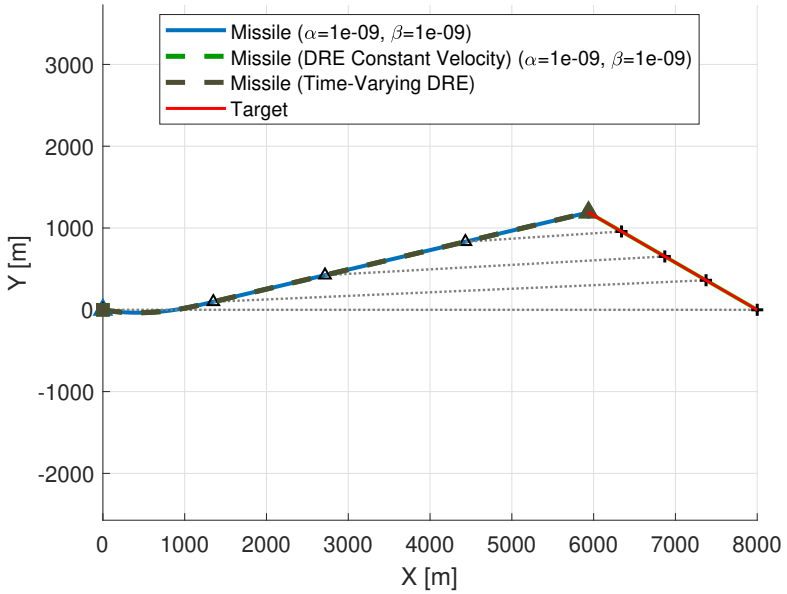

Figure 11: Missile and target trajectories comparing analytical closed-form solution with numerical time-varying Riccati integration

The flight path angle comparison in Figure 12 provides validation of the guidance law. Both the analytical and numerical implementations track the optimal reference angle ξ identically throughout the engagement, confirming that the simplified analytical expressions preserve the complete optimal control structure, including transient response and steady-state behavior.

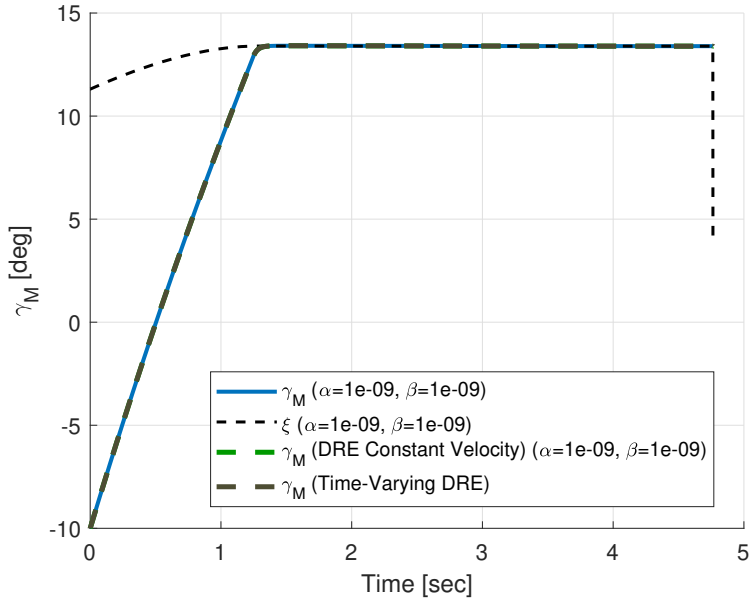

Figure 12: Flight path angle γ_M comparison between analytical and DRE solutions

Figure 13 presents the lateral acceleration control command. The acceleration profiles overlay precisely, including the initial transient correction and the subsequent near-zero steady-state performance. This perfect correspondence validates that the closed-form solution replicates the numerically computed optimal feedback gains exactly, proving the analytical solution achieves its design objective optimally and that the constant-velocity interceptor assumption is valid for the GTC strategy, where the optimal heading angle accounts for the missile's acceleration.

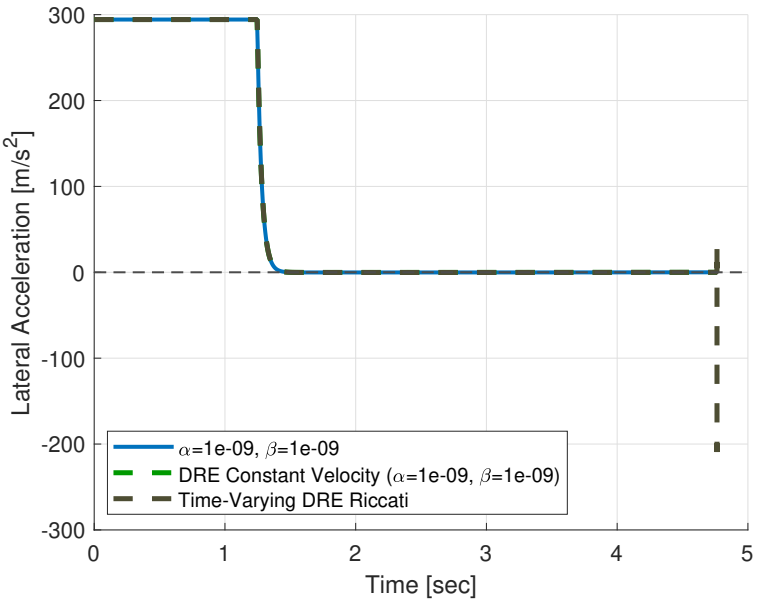

Figure 13: Lateral acceleration command comparison between analytical closed-form and numerical time-varying Riccati solutions

9 Conclusions

This project presented the derivation and validation of optimal guidance laws for interceptor missiles using the minimum variability control framework. Two distinct formulations were developed: the first addressed the problem of minimizing the variability of the body attitude angle relative to the Line-of-Sight for a TVC-equipped missile, while the second extended the framework to an augmented three-state system that enforces a terminal flight path angle constraint to achieve Guidance-to-Collision geometry.

For the first formulation, a two-stage optimization was carried out, yielding the result that the optimal guidance strategy reduces to Proportional Navigation with an effective navigation gain of $N = 2$. This gain produces a constant lateral acceleration command that nullifies the cost function entirely, independent of the weighting parameter α. The resulting law maintains a nearly constant body attitude throughout the engagement, which is valuable for system design considerations such as seeker Field-of-View limits and terminal intercept geometry. Simulation results confirmed that higher navigation gains, while still achieving interception, introduce progressively larger variations in the body angle and reduce the projection of the thrust vector along the velocity, leading to longer engagement times.

The second formulation introduced an augmented cost function that penalizes the terminal miss distance, the control effort, and the running deviation of the flight path angle from a reference collision-course angle ξ. The resulting closed-form optimal control law involves hyperbolic functions of the time-to-go through the system parameter $K = 1/(V_M\sqrt{\beta})$, and was shown to recover known guidance strategies in its limiting cases. When both weighting parameters α and β grow to infinity with a fixed ratio, the law reduces to a PN-like command driven solely by the ZEM. When both approach zero, the control is governed entirely by the heading-angle error $(\xi - \gamma_M)$, exhibiting a bang-bang behavior characteristic of the GTC strategy. These limiting cases provide physical insight into the trade-off between miss-distance minimization and flight-path-angle regulation embedded in the LQ formulation.

The reference angle ξ was determined geometrically by collapsing the collision triangle into a fourth-order polynomial in t_{go}, avoiding the computational burden of solving coupled non-linear trigonometric equations at each time step. The analytical closed-form solution was rigorously validated against a numerical time-varying Differential Riccati Equation solver using MATLAB's `ode45` integrator. Perfect agreement was demonstrated for the GTC strategy in the missile trajectories, flight path angle histories, and lateral acceleration command profiles, confirming that the closed-form expressions capture the complete optimal behavior of the GTC scheme without approximation and that real-time implementation is feasible without numerical integration overhead.

References

[1] R. Gazit and S. Gutman, "Development of guidance laws for a variable-speed missile," *Dynamics and Control*, vol. 1, pp. 177–198, May 1991.

[2] R. Gazit, "Guidance to Collision of a Variable-Speed Missile," in *Proceedings. The First IEEE Regional Conference on Aerospace Control Systems,*, pp. 734–737, May 1993.

[3] Y. Baba, M. Yamaguchi, and R. M. Howe, "Generalized guidance law for collision courses," *Journal of Guidance, Control, and Dynamics*, vol. 16, pp. 511–516, May 1993.

[4] Y.-W. Kim, B. Kim, C.-H. Lee, and S. He, "A unified formulation of optimal guidance-to-collision law for accelerating and decelerating targets," *Chinese Journal of Aeronautics*, vol. 35, pp. 40–54, July 2022.

[5] Y.-W. Kim, M.-G. Seo, and C.-H. Lee, "Investigation on energy-effective guidance-to-collision strategies for exo-atmospheric interceptors," *Aerospace Science and Technology*, vol. 124, p. 107563, May 2022.

[6] T. Shima and O. M. Golan, "Exo-atmospheric guidance of an accelerating interceptor missile," *Journal of the Franklin Institute*, vol. 349, pp. 622–637, Mar. 2012.

[7] D. Reisner and T. Shima, "Optimal Guidance-to-Collision Law for an Accelerating Exoatmospheric Interceptor Missile," *Journal of Guidance, Control, and Dynamics*, vol. 36, pp. 1695–1708, Nov. 2013.

[8] Y.-S. Jung, J.-I. Lee, C.-H. Lee, and M.-J. Tahk, "A New Collision Control Guidance Law Based on Speed Control for Kill Vehicles," *International Journal of Aeronautical and Space Sciences*, vol. 20, pp. 792–805, Sept. 2019.

[9] M. Weiss and T. Shima, "Minimum Variation Guidance Laws for Interceptor Missiles," *IFAC Proceedings Volumes*, vol. 47, no. 3, pp. 3948–3953, 2014.

[10] M. Weiss and T. Shima, "Optimal Linear-Quadratic Missile Guidance Laws with Penalty on Command Variability," *Journal of Guidance, Control, and Dynamics*, vol. 38, pp. 226–237, Feb. 2015.

[11] N. Grinfeld and J. Z. Ben-Asher, "Minimal-Jerk Missile Guidance Law," *Journal of Guidance, Control, and Dynamics*, vol. 38, pp. 1520–1525, Aug. 2015.